DEFORMATION UNFAVORABLE FOR TWIN GLIDING

EXPERIMENTAL DEFORMATION

Cylinders 1046 and 1049 were oriented unfavorably for twin gliding during deformation. Accordingly, it is instructive to compare the stress-strain curves and the deformation features produced in these tests with those for specimens 878 and 877, which were oriented favorably for twinning. Experimental conditions for deformation of the four specimens are listed in table 1, columns (1)–(5).

STRESS-STRAIN RELATIONSHIPS

Stress-strain curves for the four experiments are shown in figure 8. Although the total strain for each specimen is different, it is possible to compare the strengths of the specimens at a given percentage of strain for each set of experimental conditions. Thus, specimens 1046 and 1049 can be compared with specimens 878 and 877, respectively. At 1.7 per cent strain, specimen 1046 is 3 times as strong as specimen 878; and at 8.5 per cent strain, specimen 1049 is 1.4 times stronger than specimen 877. Both relationships are consistent with the greater strength of a calcite crystal loaded parallel to c_v, that is, in a direction unfavorable for twin gliding.

PETROGRAPHIC OBSERVATIONS AND COMPARISONS

Specimen 1046 exhibits a macroscopic shear zone or fault that is inclined at 28° to the greatest principal stress (σ_1). A fine-grained gouge of highly fractured and demolished detrital grains and pulverized calcite marks the shear zone. Detrital grains are generally slightly fractured. Grains adjacent to the shear zone are more highly fractured. The over-all fracture index is 136 (table 1, col. [7]). Nearly all the microfractures are oriented parallel to σ_1 and accordingly are extension fractures (fig. 9, *a*).

The calcite crystal in specimen 1046 contains a few *e* twin lamellae, traces of $r\{10\bar{1}1\}$ cleavage planes, and extension fractures. The twin lamellae (spacing index is 22; see table 1, col. [8]) are developed only adjacent to the macroscopic shear zone and to fractured detrital grains. Where the grains are unfractured, the calcite is untwinned. Cleavage planes ($r\{10\bar{1}1\}$) are common throughout the specimen, although they are best developed adjacent to the shear zone.[12] In addition, the calcite crystal contains fractures oriented parallel to σ_1, (fig. 9, *a*, and pl. 3*A*). The fractures are common throughout the specimen but, like the twin lamellae and *r* plates, are best developed adjacent to the shear zone. Although extension fractures in calcite are not common, they probably developed here because the crystal was loaded unfavorably for twin gliding.

It is interesting to compare the fracture indexes and twin-lamellae spacing indexes for specimens 1046 and 878 (table 1, cols. [7] and [8]). The fracture index for specimen 1046 (136) is slightly higher than that for specimen 878 (126). This probably reflects the higher strain (2.9 per cent) of specimen 1046. On the other hand, the twin-lamellae spacing index for specimen 878 (99), loaded favorably for twin gliding, is 4.5 times as high as that for specimen 1046 (22). This no doubt reflects the difference between the

[12] The possibility of translation gliding parallel to *r* cannot be excluded. Translation on *r* with a negative sense of shear is a known mechanism in calcite, and in a calcite crystal compressed parallel to c_v, there is a high resolved shear stress parallel to *r* planes and in the correct sense for translation gliding. However, since translation gliding does not produce visible lamellae, and since there has been no internal rotation, it cannot be substantiated.

PLATE 2

A, Cluster of sand crystals.

B, Orientation of principal stresses during deformation is shown in center of figure. In *a*, *b*, *c*, and *d*, planar microfractures are illustrated that are developed in parallel sets oriented perpendicular to σ_3 and parallel to σ_1; i.e., they are extension fractures. In *c*, a microshear zone in a feldspar grain is shown. The shear zone is inclined at 30° to σ_1. In *b* and *d*, twin lamellae in the calcite crystals are visible. Crossed nicols.

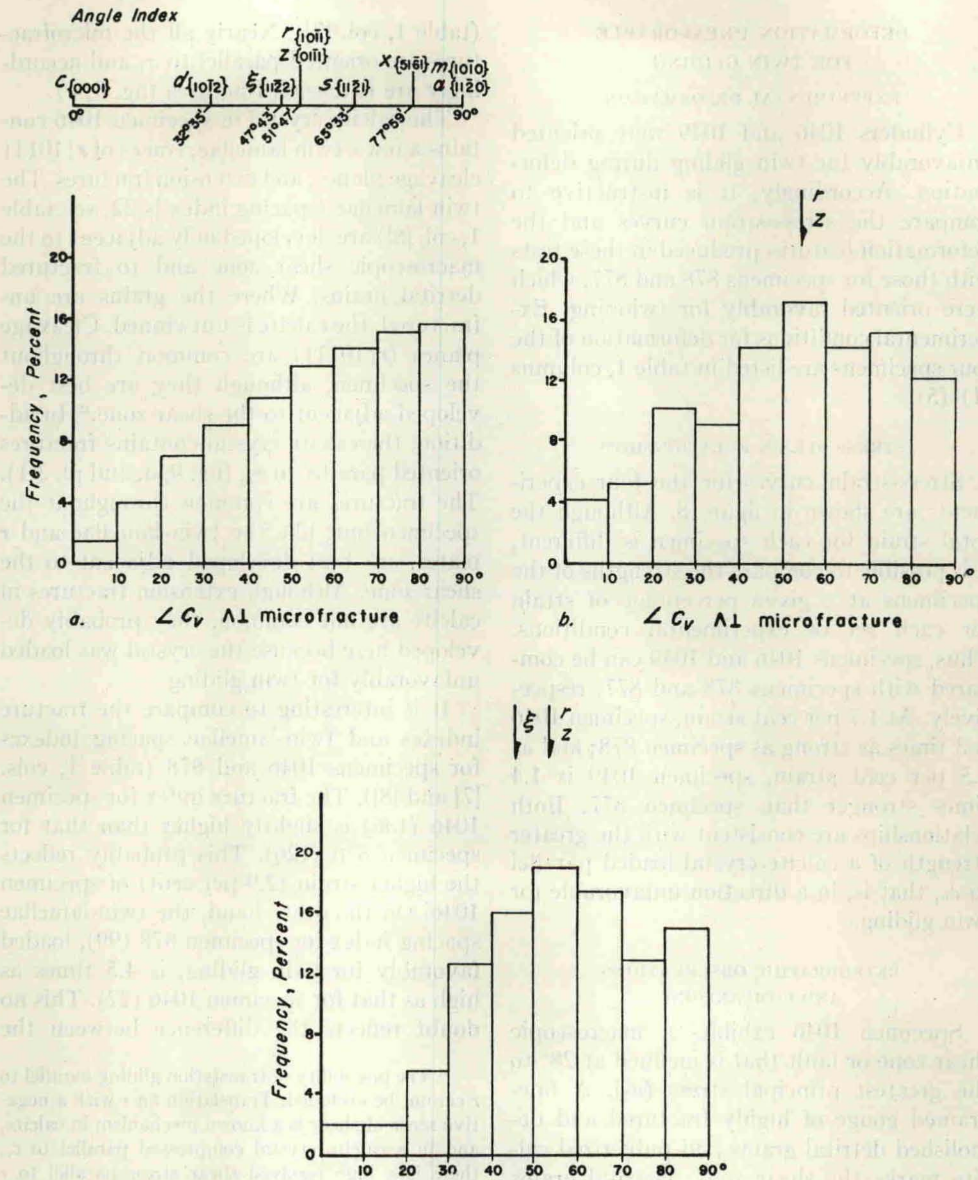

FIG. 6.—Histograms of distribution of angles between normal to microfractures and c_V in host quartz grains. *a*, random distribution (Bloss, 1957):

$$P = 100 \int_{\theta_1}^{\theta_2} \sin\ \theta d\theta = 100(\cos\ \theta_1 - \cos\ \theta_2)$$

$$\theta_2 - \theta_1 = \text{cell width in degrees}\ .$$

Angle index shows angles between c_V and common forms in quartz. (This index applied to all diagrams of fig. 6.) *b*, specimen 911; data are from 111 fracture sets in 100 quartz grains. *c*, specimen 725. Data are from 348 fracture sets in 200 quartz grains.